# Energy balance for single or multiple droplet chains impinging onto a hot slab in the Leidenfrost regime

P. Dunand, G. Castanet, F. Lemoine, D. Maillet, M. Gradeck
LEMTA CNRS, University of Lorraine, France
michel.gradeck@univ-lorraine.fr and guillaume.castanet@ensem.inpl-nancy.fr

**Abstract**

This work aims at estimating the energy balance of a single droplet chain or multiple droplet chains impinging onto a hot wall whose initial temperature is above the Leidenfrost point. The experimental data (temperature of incoming and outcoming droplets, heat flux at the wall,…) are required for validating submodels for heat transfer between a hot wall and sprays. Indeed, these physical submodels are subsequently used in CFD modeling. In the Leidenfrost regime, impinging droplets can experience only three different regimes : perfect bouncing, bouncing with a satellite formation and splashing. Modeling heat transfer in these regimes requires the knowledge of several parameters such as the spreading diameter, heat transfer at the wall, the thickness of the vapour layer, its temperature as well as the liquid heating during the impingement and the evaporation rate. In the splashing regime, data about secondary droplets are also required. Up to now, no experimental data base giving all these parameters are available because of the difficulty to measure simultaneously all these parameters. In this experimental work, some of these parameters have been measured simultaneously during the interaction of the droplet with the heated wall while other ones have been estimated by means of an energy balance.

## Introduction

In this study, the focus is placed on non wetting conditions; the wall temperature is above the Leidenfrost temperature, which corresponds to the film boiling regime. A thin vapor layer forms quasi-instantaneously between the droplet and the wall and prevents the droplet to stick the wall. The splashing and the rebound of the droplets are thus the only behavior that can occur. The rebound regime is observed for low Weber number while an increase of the Weber number promotes the splashing, Rein [1]. When metallurgical heat treatments are considered, e.g. in steel industry, film boiling is the dominant regime. An ideal quench is one that proceeds at an infinitely fast rate; however the vapor cushion between the droplet and the solid insulates the droplet from the hot sample and thus limits drastically the heat transfer, Bernardin and Mudawar [2]. For the cases of the rebound and splashing regimes, velocity of the outcoming droplets has been widely investigated, Wachters et al. [3]; Schmell et al. [4], Mundo et al., [5]. In the same way, post-impact droplets size distribution has been widely investigated in the literature, for temperatures greater than the Leidenfrost limit [6] or above [4]. To the best of our knowledge, there is no data in the literature related to the post-impact droplet temperature except the recent works of Castanet et al. [7] and Dunand et al. [8].

In the present work, different measurement techniques are combined for an indirect estimate of the mass of liquid evaporated during the droplet/wall interaction. The temperature variation of the droplet is measured using the two-color planar laser-induced fluorescence thermometry. In addition, an infrared camera provides the temperature field at the rear face of the nickel target. A semi-analytical inverse heat conduction model allows estimating the heat flux on the front face of the plate where the droplets impinge. Finally, the heat flux removed from the wall by the droplets is compared to the sensible heat stored in the outgoing droplets. Energy conservation is finally invoked to estimate the heat flux associated to evaporation. The respective contributions of the liquid sensible heat, the heat of evaporation, and the heat removed from the wall are analyzed in terms of incident droplet size and normal Weber number.

## Droplet generation and experimental set-up

In order to study droplet/wall interactions, an experimental set-up was specifically designed. A sketch of the experimental set-up is shown in figure 1. In this study, the droplets range from 80 µm to 250 µm while their velocity is of the order of a few m/s. The droplet generator can be rotated to any prescribed angle $\alpha$ of incidence. The temperature of the injector body is regulated and the liquid temperature is controlled by a thermocouple placed just before the outlet of the injector. Water droplets impact periodically a thin disc of nickel (thickness is 500 µm and radius R=12.5mm) which is heated by electromagnetic induction. In this contactless heating technique, the distribution of the heat sources in the skin depth of the metallic sample is perfectly controlled. The low thickness of the nickel disc allows limiting the damping of the thermal response at the rear face (side of the sam-

ple opposite to the droplet impact). This nickel sample is put on three ceramic spheres (at the radius Rc) in order to ensure a better insulation from the solid support. The upper surface of the nickel on which the droplet are impacting, is polished as a mirror. An oxide layer covers the surface when the temperature exceeds 500°C. This green and gray layer is very stable, and did not provide a significant change in the overall roughness. In addition, the oxidation increases the radiative emissivity of the wall, which is positive in turn for the infrared thermography.

**Measurement techniques**

**→ Measurements of the droplets size and velocity by shadowgraphy**

A high-speed (HS) camera is used to visualize droplets impinging onto the heated wall. The HS camera is a Phantom v710 equipped with a 12-bits CMOS sensor that can provide up to 7500 fps at full resolution (1280×800 pixels). It is used with a reduced resolution to perform the image acquisition at a much higher frame rate, typically in the order of 100,000 fps. This acquisition rate is sufficient to resolve in time the droplet/wall interactions in the experimental conditions encountered in this study. The droplets are backlighted using a very bright light source (a 400 W HMI lamp with a parabolic reflector). A zoom lens allows having a field of view ranging from 400 µm to 3 mm. The images are then processed with a homemade detection and tracking software in order to determine the main features of the incoming and outcoming droplets. The tracking algorithm is based on a multi-hypothesis tracking method, Reid [9]. Joint distributions of the droplets size and velocity can be derived from the processing of the images. Other important parameters such as the incident angle, the normal and tangential velocities, the residence time, or the spreading diameter of the droplets can be also extracted concomitantly.

**→ Two-colour Planar Laser-Induced fluorescence thermometry**

The two-color planar laser-induced fluorescence (2cPLIF) was used to measure the variation in the droplet temperature during their interaction with the wall. This technique already demonstrated its ability to characterize the temperature of droplets in various situations including droplet evaporation in either inert or reactive flows, Castanet et al. [10]; Depredurand et al. [11]. It was also used to determine the droplet change in temperature during their impingement onto a heated solid surface, Castanet et al. [7]. In this study, the 2cLIF thermometry was restricted to pointwise measurements, which imply a cumbersome point-by-point scanning to reconstruct the temperature distribution in the liquid phase of the flow. More recently, the technique was extended to planar laser induced fluorescence (PLIF) in order to obtain the temperature field, Dunand et al., [8]. The 2cLIF thermometry is based on the measurement of the fluorescence intensity of a single dye tracer. In liquids, the fluorescence quantum yield is strongly influenced by the quenching, which depends on the temperature. When a laser beam induced the fluorescence of a dye dissolved into a liquid, the fluorescence signal detected on a given spectral band *i* can be expressed as (Lavieille et al. [12]; Castanet et al. [9]):

$$I_{f,i} \approx K_{opt,i}\, K_{spec,i}\, I_0\, cV \exp\left(\frac{\beta_i}{T}\right),\ i=1,2 \qquad (1)$$

where $K_{opt,i}$ is a parameter depending on the optical properties of the detection system (e.g. the solid angle of the detection, the spectral sensitivity of the detectors, the spectral band of detection), $K_{spec,i}$ is a parameter depending on the spectroscopic properties of the tracer in its solvent on the designated spectral band. c is the concentration in dye molecules and the product c. $V$ corresponds to the number of molecules that are illuminated by the laser beam in the field of view of the detector. $I_0$ is the intensity of the laser beam before crossing the absorbing medium. $\beta_i$ are parameters related to the temperature sensitivity of the fluorescence signal. In this study, rhodamine 640 was selected as a fluorescent tracer. The ratio of the fluorescence intensity measured on two bands, for which the temperature sensitivity is highly different ([12] and[8]), allows eliminating the effects of parameters that are unknown or difficult to control. When the technique is applied in imagery, only the coefficients do not depend on the pixel position in the image. All other variables can change from one pixel to another, especially the parameter $K_{opt,i}$. Even under isothermal conditions, the fluorescence ratio is not necessarily uniform, due mainly to the non-uniformity of the CCD detection matrix. To eliminate the influence of the detection system, a reference image at a known temperature $T_0$ (with the same optical configuration as for the measurement) is recorded. According to equation (1), denoting $R_0$ the fluorescence ratio obtained in the reference measurement, the temperature can be derived from the ratio of fluorescence field.

$$\ln\left(\frac{R_f}{R_0}\right) = (\beta_1 - \beta_2)\left(\frac{1}{T} - \frac{1}{T_0}\right),\ i=1,2 \qquad (2)$$

where $R_f = I_{f1}/I_{f2}$ and $R_0 = I_{f10}/I_{f20}$ .

Once $\beta_1$ and $\beta_1$ are known, equation (2) can be used to determine the liquid temperature. The bands of detection correspond to the ranges [555 nm-565 nm] and [635 nm-685 nm]. The variation of the fluorescence ratio $R_f$ is about 1.4%/K which is enough in practice to measure the droplet temperature with an accuracy of about 2°C.

The measurement system is illustrated in figure 2. The excitation of Rh640 is achieved by means of a Cw Nd:YAG laser (Laser Quantum Finesse, 6W @532 nm). An arrangement of spherical and cylindrical lenses provides a laser sheet with a thickness of 220 µm and a height of 16 mm in the measurement zone. This latter is observed by a Questar QM-1 long distance microscope, which is positioned perpendicularly at a working distance of about 84 cm. The field of view is then about 3.5x3.5 mm². A holographic filter (Notch Plus, Kayser Optical) is used to block the Mie scattering of the laser light at 532 nm. A neutral beamsplitter (R/T 45/55%) allows splitting the fluorescence signal for its acquisitions by the cameras. Interference filters are mounted in front of the cameras and allows selecting the aforementioned spectral bands. For the detection of the fluorescence images, two electron-multiplying CCD cameras (Hamamatsu EM-CCD camera C9100-02- 14 bits) with a spatial resolution of 1000x1000 pixels are used. The measurements are performed with a concentration in Rh640 equal to $5.10^{-5}$ mol/L. This concentration is relatively high and the re-absorption of the fluorescence within the droplet cannot be ignored. However, this high concentration is required to limit the effect of the droplet size and shape on the fluorescence spectrum which has been described by Labergue et al. [13]. The re-absorption of the fluorescence is likely to modify differently the fluorescence ratios of incoming and outcoming droplets only in the case of a splashing. In the case of a rebound, the droplet does not change significantly in diameter. Re-absorption of the fluorescence can be accounted for in the case of a splashing. The extinction coefficients of each spectral band being known, the fluorescence ratio can be corrected by:

$$R_{fcor} = R_f.\mu = \frac{\int_{\vartheta} I_{f_1}(\vec{x})\exp(-\varepsilon_1\vec{x})\,d\vartheta}{\int_{\vartheta} I_{f_2}(\vec{x})\exp(-\varepsilon_2\vec{x})\,d\vartheta} \tag{3}$$

In this expression, µ is a correction factor taken into account the effect of absorption, $\vec{x}$ is a given position in the droplet and $\vartheta$ is the droplet volume. In the case of a splashing, only the ratio corresponding to droplet before impact is corrected. The sizes of the secondary droplets are generally too small to be significantly influenced by the re-absorption of the fluorescence. For a 200 µm, the applied correction is on the order of 2.78°C and it decreases to 1.47°C when the diameter is 100 µm.

Figure 3 shows an example of measurement in the case of a splashing and figure 4 in the case of rebound. A significant heating of the droplets resulting from their impingement is observed. The fluorescence field is not uniform in an image; this is mainly related to the time averaged liquid concentration, which varies strongly in space. The liquid concentration is the more important near the impact region where the droplet are strongly squeezed. From these images of the temperature field, the average temperature of primary and secondary droplets can be calculated. The average is weighted by the fluorescence intensity since this latter is roughly proportional to the liquid mass flow rate crossing the region of interest (ROI) during the integration time of the cameras:

$$T_m = \iint_{ROI} T(x,y)\,I_f(x,y)\,dx\,dy \Big/ \iint_{ROI} I_f(x,y)\,dx\,dy \tag{4}$$

ROI are defined for the incident droplets and the secondary droplets. The difference in temperature $\Delta T_l$ between these regions is finally computed and allows evaluating the gain of sensible heat of the liquid.

**→ Infrared thermography and inverse conduction model for the wall heat flux estimation**

In all the experiments, the nickel sample (R=12.5mm and thickness e = 500µm) is first heated up to 700-750°C. Then heating is stopped and cooling by the water droplets stream occurs. As the slab is impacted by the droplets on one of its face (referred as "front face"), the temperature field is measured on the other face (referred as "rear face") using an IR camera in the spectral range [3.97-4.01µm]. Acquisitions are performed at sampling frequency of 60 Hz and at maximum resolution of 320x240 pixels. A specific inverse heat conduction algorithm was developed to recover the heat flux removed from the front face corresponding to droplets impacts. Our method is based on an analytical solution of the heat equation using integral transforms.

- *Solution of the direct heat transfer problem*

The internal transient conduction within the Ni disc is considered. As the resident time of each droplet is very low compared to the time associated with the sampling frequency of the IR camera, an averaged value of the heat flux over the resolution time of the camera (or a multiple of it) will be inferred from the measurements. In order to decrease the number of unknowns associated with the heat flux distribution, the 3D modelling is re-

duced to a 2D modelling through angular averaging in a cylindrical coordinate system. Then, assuming constant thermophysical properties, the following set of equations is obtained:

$$\frac{\partial^2 T}{\partial r^2}+\frac{1}{r}\frac{\partial T}{\partial r}+\frac{\partial^2 T}{\partial z^2}=\frac{1}{a}\frac{\partial T}{\partial t} \tag{5}$$

$$T\,(r,\,z,\,t=0)=T_{init}\,(r) \tag{6}$$

$$-\lambda\left.\frac{\partial T}{\partial r}\right|_{r=0}=0 \quad and \quad -\lambda\left.\frac{\partial T}{\partial r}\right|_{r=R}=0 \tag{7}$$

$$\lambda\left.\frac{\partial T}{\partial z}\right|_{z=0}=q_F \quad and \quad -\lambda\left.\frac{\partial T}{\partial z}\right|_{z=e}=q_R \tag{8}$$

$$\text{with: } q_F=h_{EQ}^F\left(T_F-T_\infty\right)+q_d\left(r,\,t\right) \quad \text{and} \quad q_R=h_{EQ}^R\left(T_R-T_\infty\right)+K_{cond}\,\delta(r-R_c)\left(T_R-T_{stum}\right). \tag{9}$$

$h_{EQ}^\beta$ corresponds to the heat loss coefficient which is the sum of both convective and radiative losses over the rear ($\beta = R$) and front ($\beta = F$) faces of the disc. $q_d$ is the heat flux removed from the front face by the droplet stream. It is averaged angularly over a circle at radius $r$ . $T_\infty$ is the air temperature and $T_F$ and $T_R$ are the front and rear face temperatures, $T_{init}$ is the initial temperature field and $T_{stum}$ the temperature of the support (three insulating beads placed at 120° and a radius $R_c$ in between the Nickel disc and a hollow cylindrical support built in stumatite. $K_{cond}$ is a conductance between sample and support. Convective contributions to $h_{EQ}^\beta$ have been calculated using natural convection correlations over horizontal surfaces. Linearized radiative contributions to $h_{EQ}^\beta$, the radiative transfer coefficients, differ since the front face radiative environment is the ambient while the rear face is coupled with both the ambient and the stumatite support. All these coefficients have been estimated thanks to a relaxation experiment in the absence of any droplet stream.

The Laplace ($^-$) and Hankel ($\sim$) transforms are used so that equation (5) becomes :

$$\frac{\partial \bar{\tilde{\theta}}_n^2}{\partial z}-(\alpha_n^2+\frac{p}{a})\;\bar{\tilde{\theta}}_n=0\,, \tag{10}$$

where $\theta = T - T_{init}$, $p$ is the Laplace parameter, $\alpha_n = u_n / R_d$, $u_n$ solutions of $J_1(u_n)=0$ and:

$$\tilde{\theta}_n\,(z,t)=\int_0^R \theta\,(r,t,z)\;r\;\mathrm{J}_0(\alpha_n r)\;\mathrm{d}r \qquad ; \qquad \bar{\tilde{\theta}}_n\,(p,z)=\int_0^\infty \tilde{\theta}_n\,(z,t)\;\mathrm{e}^{-pt}\;\mathrm{d}t \tag{11}$$

Finally, the quadrupole method (Maillet et al.[14]) yields a linear relationship between the rear face temperature ($z = e$) and the cooling heat flux ($z = 0$) :

$$\bar{\tilde{\theta}}_n^{\,R}\,(p)=-\bar{\tilde{Z}}_n\,(p+a\,\alpha_n^2)\;\tilde{\bar{q}}_{n,d}\,(p)+\bar{\tilde{W}}_n^{\infty}(p+a\,\alpha_n^2)\;\tilde{\theta}_{n,\infty}-\bar{\tilde{W}}_n^{stum}(p+a\,\alpha_n^2)\left[p\;\bar{\theta}\,(R_c,p)-\tilde{\theta}_{n,stum}\right] \tag{12}$$

with

$$\bar{\tilde{Z}}_n\,(p)=\left[(h_{EQ}^F+h_{EQ}^R)\cosh(k\,e)+\left(\frac{h_{EQ}^F\,h_{EQ}^R}{\lambda\,k}+\lambda\,k\right)\sinh(k\,e)\right]^{-1}, \tag{13}$$

$$\bar{\tilde{W}}_n^{\infty}\,(p)=\left(\cosh(k\,e)+\frac{h_{EQ}^F}{\lambda\,k}\sinh(k\,e)\right)\frac{h_{EQ}^R}{p}\,\bar{\tilde{Z}}_n\,(p) \tag{14}$$

$$\bar{\tilde{W}}_n^{\,stum}\,(p)=K_{stum}\,R\,R_c\,\frac{\mathrm{J}_0(\alpha_n\,R_c)}{p}\,\bar{\tilde{Z}}_n\,(p) \tag{15}$$

Numerical Laplace inversion of the previous expressions allows calculating the Hankel transform of the rear face temperature field at any time:

$$\begin{aligned}\tilde{\theta}_n^{\,R}\,(t)=&\int_0^t \exp(-\alpha_n^2\,(t-t'))\;\tilde{\mathrm{Z}}_n\,(t-t')\;\tilde{q}_{n,d}\;(t')\;\mathrm{d}t'+\exp(-\alpha_n^2\,t)\;\tilde{W}_n^{\infty}\,(t)\;\tilde{\theta}_{n,\infty}\\&-\exp(-\alpha_n^2\,t)\;\tilde{W}_n^{\,stum}\;\tilde{\theta}_{n,stum}\,(t)+\int_0^t \exp(-\alpha_n^2\,(t-t'))\;\tilde{W}_n^{\,stum}\,(t-t')\;\frac{\partial\theta^R}{\partial t}(R_c\,,t')\;\mathrm{d}t'\end{aligned} \tag{16}$$

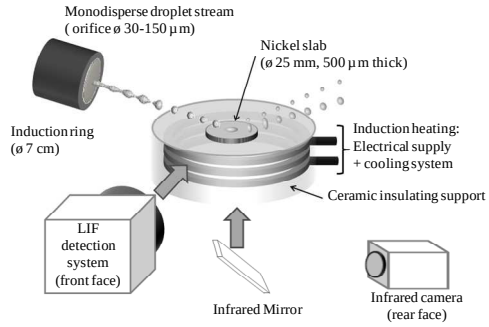


**Figure 1** Experimental set-up

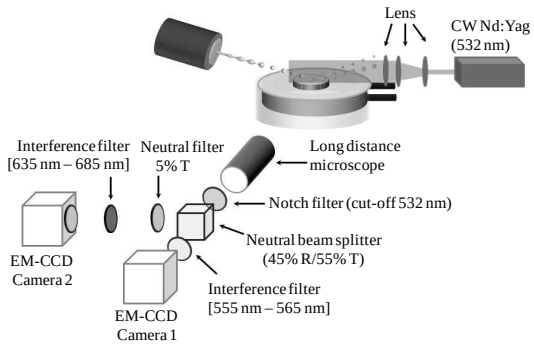


**Figure 2** 2cPLIF optical set-up

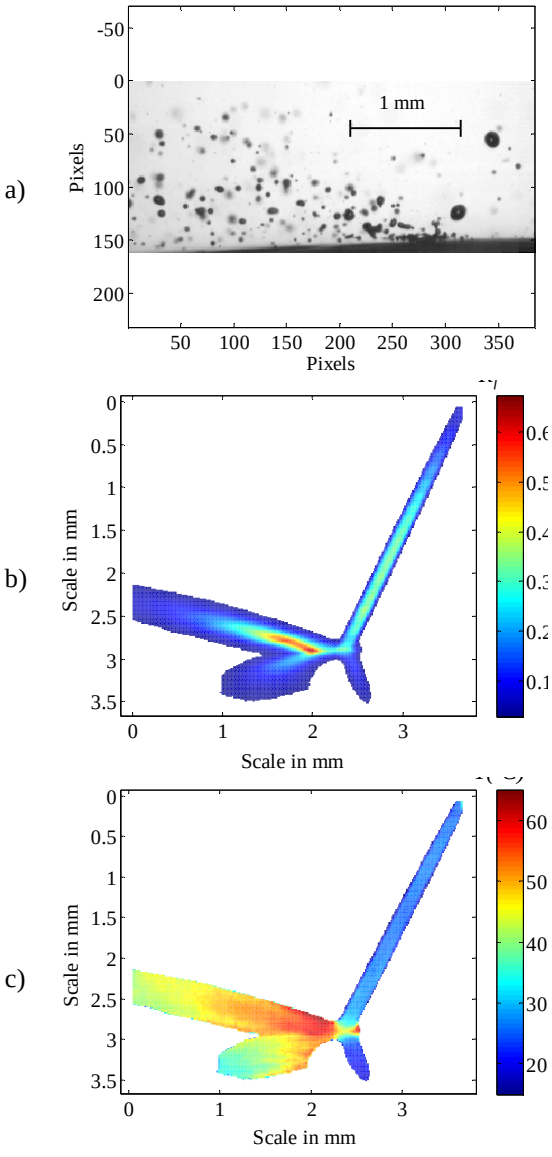


**Figure 3** example of 2cPLIF measurement in the case of a splashing ($D$=180 µm, $V_d$=10 m/s, $\alpha$=70.3°, $f$=12 kHz, $T_w$=540°C) (a: shadow image, b: fluorescence intensity field on camera 1 (555-565nm), c: resulting temperature distribution)

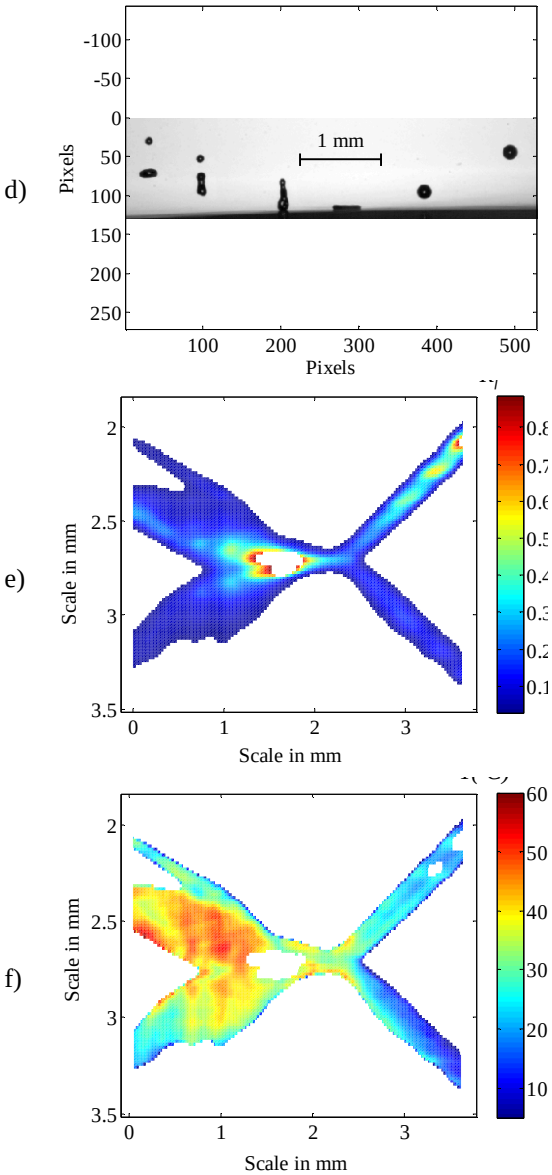


**Figure 4** example of 2cPLIF measurement in the case of a rebound with satelite droplets ($D$=133µm, $V_d$=10.5 m/s, $\alpha$=24.2°, $f$=12.5kHz, $T_w$=670°C) (d: shadow image, e: fluorescence intensity field on camera 1 (555-565nm), f: resulting temperature distribution)

The real temperature in the time-space domain can be finally obtained through the Hankel inversion of the previous equations:

$$\theta^R(r,\,t_k) = \frac{2}{R^2}\sum_{n=0}^{nh}\frac{\mathrm{J}_0(\alpha_\mathrm{n}\,r)}{\mathrm{J}_0^2(\alpha_\mathrm{n}\,R)}\,\tilde{\theta}_n^R(t_k)\,. \tag{17}$$

- **Inverse heat transfer problem**

Temperature at the rear of the wall $T^R(x, y, t)$ is measured by the infrared camera in a Cartesian reference frame while the input data $T^R(r,t)$ of the model must be known in a cylindrical reference frame. Thus, it requires the conversion and the averaging of the initial Cartesian temperature field in order to obtain the input data. As a consequence, only an averaged heat flux $q_R(r, t)$ can be obtained, but not the local heat flux $q_R(x, y, t)$. The first step of the inversion procedure consists in obtaining the input temperature by angular averaging the initial field.

$$\boldsymbol{\theta}^R(r_m,t_k) = \frac{2}{R^2}\sum_{n=0}^{nh}\frac{\mathrm{J}_0(\alpha_n\,r_m)}{\mathrm{J}_0^2(\alpha_n R)}\,\theta_n^R(t_k) \Rightarrow \boldsymbol{\theta}^R(t_k) = \boldsymbol{X}\,\tilde{\boldsymbol{\theta}}(t_k)\,, \tag{18}$$

where $\boldsymbol{\theta}^R(t_k)$ is the column vector of the rear face temperature differences for all observable pixels, of size $n_x$ $n_y$ and $\tilde{\boldsymbol{\theta}}(t_k)$ the column vector composed of its Hankel harmonics of orders 0 to *nh*.

Equation (16), expressed in Hankel domain (~), is the second step of the inverse heat conduction problem (IHCP); the integral form can be expressed using a quadrature :

$$\begin{aligned}\tilde{\theta}_n^{cor}(t_k) &= \tilde{\theta}_n^R(t_k) - exp(-\alpha_n^2\,t_k)\,\tilde{W}_n^{\infty}\;\tilde{\theta}_{n,\infty}(t_k) = \sum_{j=1}^{k} exp\left(-\alpha_n^2\,t_{k-j+1}\right)\tilde{Z}_n(t_k)\,\tilde{q}_{n,d}(t_j)\Delta t \\ &= \sum_{j=1}^{k} S_{kj}\;\tilde{q}_{n,d}(t_j)\Delta t\end{aligned}\,, \tag{19}$$

where $\Delta t$ is the time step of the infrared camera (1/60 s here). It is the time regularization hyperparameter that has been chosen not too high, in order to get unbiased estimates of temperature and flux and not too low to prevent an explosion of the inversion because of the presence of noise in the temperature measurements.

Calling $\tilde{\boldsymbol{\theta}}_n^{cor\,exp}$ the vector of the $n^{\text{th}}$ harmonics of the corrected experimental rear face temperature, calculated according to (19) and a least square inversion results from model (19):

$$\hat{\tilde{\boldsymbol{q}}}_{n,d} = \left(\boldsymbol{S}^T\,\boldsymbol{S}\right)^{-1}\boldsymbol{S}^T\,\tilde{\boldsymbol{\theta}}_n^{cor\,exp}\,. \tag{20}$$

Estimation of the wall flux $q_d$ is then made using a truncation of its spectrum to a maximum of *nh* + 1 harmonics:

$$\hat{q}_d(r,\,t_k) = \frac{2}{R^2}\sum_{n=0}^{nh}\frac{\mathrm{J}_0(\alpha_\mathrm{n}\,r)}{\mathrm{J}_0^2(\alpha_\mathrm{n}\,R)}\,\hat{\tilde{q}}_{n,d}(t_k) \tag{21}$$

In practice, only two harmonics ($n$ = 0 and 1) are used, because of the weakly local effect of the droplet stream on the rear face temperature field (the disc is thin and highly diffusive). This number is the hyperparameter for space regularization. The total rate of heat flow $\dot{Q}_d(t)$ is estimated by:

$$\hat{\dot{Q}}_d(t_k) = 2\pi\int_0^R \hat{q}_d(r,t_k)\,r\,\mathrm{d}r = 4\pi\sum_{\mathrm{n}=0}^{nh}\frac{\mathrm{J}_1(\alpha_\mathrm{n}\,r)}{\alpha_\mathrm{n}R\,\mathrm{J}_0^2(\alpha_\mathrm{n}\,R)}\,\hat{\tilde{q}}_{n,d}(t_k) \tag{22}$$

Finally, the energy removed from the wall at each droplet impact is computed from (21) knowing frequency $f_{inj}$ of the injector of the droplet stream:

$$Q_w(t) = \frac{\dot{Q}(t)}{f_{inj}} \tag{23}$$

More details about the previous modelling can be found in Gradeck et al. [15] and Maillet et al. [16].

**Energy balance of the droplet/wall interaction**

The energy balance of the droplet/wall interaction can be written as the sum of three contributions, the sensible heat gained by the liquid, the phase change heat and the heat drained by the vapour flow:

$$Q_w = Q_l + \Delta m\cdot\left(L_v + Cp_v\Delta T_v\right) \tag{24}$$

In this expression, the term $Cp_v\ \Delta T_v$ corresponds to the sensible heat drained by the vapor, where $\Delta T_v = T_f - T_b$ is the vapour temperature increase. $Q_l$ corresponds to the sensible heat gained by the liquid. It can be expressed as follows :

$$Q_l = \left[ (m-\Delta m) Cp_l \Delta T_l + \Delta m Cp_l (T_s - T_{inj}) \right] \quad (25)$$

In these expressions, $\Delta m$ is the mass of the droplet evaporated during its impingement, $\Delta T_l$ is the increase in the liquid temperature measured by 2cLIF thermometry.

The parameters $T_s$ and $\Delta T_v$ are not measured but in a first approach, $T_s$ can be replaced by the boiling temperature of the liquid and $\Delta T_v$ can be estimated by assuming $\Delta T_v = T_f - T_b$. Introducing the Jakob number $Ja = Cp_v \Delta T_v / L_v$ :

$$Q_w = Q_l + L_v \Delta m\ (1+Ja) \quad (26)$$

Finally, the mass of the droplet evaporated during its interaction with the wall can be expressed by:

$$\Delta m = \frac{Q_w - m Cp_l \Delta T_l}{L_v (1+Ja) + Cp_l (T_b - T_{l,f})}, \quad (27)$$

where $T_{l,f}$ is the temperature of the liquid after the impingement.

Figure 5 shows the evolution of $\Delta m/m$ as function of the Weber number, for different droplet sizes. We observed that this parameter varies strongly with the droplet size. For the smallest droplets ($D$=80 µm), the relative variation in mass is very significant as it can reach about 25%, while it is negligible for the largest droplets. As expected, due to the increase in spreading diameter, $\Delta m/m$ is increasing with the Weber number.

The cooling efficiency $\varepsilon$ can be written:

$$\varepsilon = \left(Q_l + \Delta m(1+Ja)\right) \Big/ \left[ m\left(L_v + Cp_v\left(T_f - T_b\right)\right)\right] \quad (28)$$

Introducing $L_{ve} = L_v + Cp_v\left(T_f - T_b\right) = L_v\left(1+Ja\right)$,

$$\varepsilon = \frac{Q_l}{mL_{ve}} + \frac{\Delta m}{m}. \quad (29)$$

This equation shows the respective contributions of the sensible heat and the evaporation to the cooling efficiency. These contributions are compared in figure 6. For the biggest droplets, the dominant contribution is related to the sensible heat. For the smallest droplet, it is the contrary. This result is particularly interesting for the modelling of spray cooling since it points out the interest of taking into account the sensible heat gained by the liquid. Sensible heating is often neglected while its contribution to the cooling is a matter of droplet size and secondarily of Weber number.

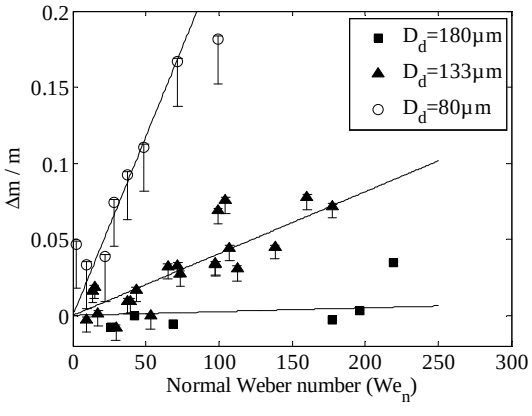


**Figure 5.** Evolution of the relative loss of mass $\Delta m/m$ as a function of the normal Weber number for different droplet sizes ($f$ ranges from 9500 Hz to 12000 Hz).

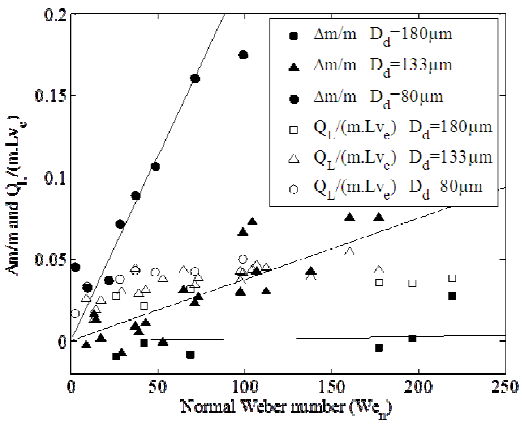


**Figure 6.** Comparison between $\Delta m/m$ and $Q_L/mLv_e$ ($f$ ranges from 9500 Hz to 12000 kHz).

## Conclusion

The implementation of innovative non-intrusive diagnostics allows investigating the different contributions to the energy balance in the Leidenfrost effect.

Infrared thermography combined with an inverse heat conduction model allowed estimating the heat flow rate removed from the wall by the impact of monodisperse droplet streams and consequently the heat removed per droplet.

Furthermore, 2cPLIF thermometry was used to measure the increase in the temperature of the droplets during an impact and thus to determine the sensible heat gained by the liquid. The contribution of evaporation to the wall cooling was obtained from the closure of the energy balance. The main interest of this approach is that it is almost impossible to quantify directly the mass of liquid after the impact, since the droplets can be strongly deformed after impinging the wall. It was clearly observed that the main contribution to the cooling is the gain of sensible heat by the liquid in the case of the large droplets. When the droplet size decreases, the heat removed by evaporation becomes dominant. In all the cases, heat transfers increase with the normal Weber number. A better assessment of the evaporated mass would require quantifying the enthalpy of the vapor trapped between the droplet and the wall.

## Acknowledgements

This work has been supported by the French National Agency (ANR) in the frame of the research program IDHEAS (ANR-NT09 432160)

## References

[1] Rein, M., 2002. *Drop-surface interactions*, Wien New York: Springer.

[2] Bernardin, J. D., Mudawar, I., 1997. *Mapping of impact and heat transfer regimes of water drops impinging on a polished surface* . Int. J. of Heat and Mass Transfer. 40, 2579-2593.

[3] Wachters, M.M.J., Westerling, N.A.J., 1966. *The heat transfer from a hot wall to impinging water drop in the spheroidal state*. Chemical. Eng. Sciences. 21, 1047-1056.

[4] Schmehl R., Rosskamp H., Willmann M., Wittig S., 1999. *CFD analysis of a spray propagation and evaporation including wall film formation and spray/film interactions*. Int. J. of Heat and Fluid Flow. 20, 520-529.

[5] Mundo, C.HR., Sommerfeld, M., Tropea, C., 1995. *Experimental studies of the deformation and break-up process*. Int. J. of Multiphase Flow. 21, 151-173.

[6] Dewitte J., Berthoumieu P., Lavergne G., 2005. *An experimental study of droplet hot wall interactions and a survey of the splashing regime*. 5th Int. Symp. on Multiphase Flow, Heat Mass Transfer Energy Conversion, Xi'an, China.

[7] Castanet, G., Liénart, T., Lemoine, F., 2009. *Dynamics and temperature of droplets impacting onto a heated wall*. Int. J. of Heat and Mass Transfer. 52, 670-679.

[8] Dunand, P., Castanet, G., Lemoine, F., 2011, in 15th Int. Symp. on Applications of Laser Techniques to Fluid Mechanics, Lisbon, Portugal.

[9] Reid, D.B., 1979. *An algorithm for tracking multiple targets. IEEE Transactions on Automatic Control*. 24, 843-854.

[10] Castanet, G., Lavieille, P., Lebouche, M., Lemoine, F., 2003. Measurement of the temperature distribution within monodisperse combusting droplets in linear streams using two-color laser-induced fluorescence. Exp. in Fluids. 35, 563-571.

[11] Deprédurand, V., Castanet, G., Lemoine, F., 2010. *Heat and mass transfer in evaporating droplets in interaction: Influence of the fuel*. Int. J. of heat and mass transfer. 53, 3495-3502.

[12] Lavieille, P., Delconte, A., Blondel, D., Lebouché, M., Lemoine, F., 2004. *Non-intrusive temperature measurements using three-color laser-induced fluorescence*. Exp. in Fluids. 36, 706-716.

[13] Labergue, A., Deprédurand, V., Delconte, A., Castanet, G., Lemoine, F., 2010. *New insight into two-color LIF thermometry applied to temperature measurements of droplets*. Exp. in Fluids. 49, 547-556.

[14] Maillet, D., André, S., Batsale, J. C., Degiovanni, A., Moyne C., 2000. *Thermal Quadrupoles. Solving the heat equation through integral transforms*. John Wiley & Sons Ed 2000.

[15] M. Gradeck, F. Lelong, N. Seiler, D. Maillet, *How to estimate the heat transfer due to droplets impinging onto a hot slab?*, 2009, ExHFT-7, Krakow 2009 (Poland)

[16] Maillet, D., Gradeck, M., Rémy, B., Ouattara, A., Lelong, F., 2010. *Inverse conduction technique in Hankel domain using infrared thermography: application to droplet stream quenching a metal disk*. 14th Int. Heat Transfer Conf., Washington DC, USA.